POLITECNICO DI TORINO
Repository ISTITUZIONALE

Passenger car active braking system: Pressure control design and experimental results (part II)

Publisher copyright

(Article begins on next page)

30 April 2024

Passenger Car Active Braking System: pressure control design and experimental results (Part II)

Antonio Tota, Enrico Galvagno, Mauro Velardocchia, and Alessandro Vigliani

antonio.tota@polito.it, enrico.galvagno@polito.it, mauro.velardocchia@polito.it, alessandro.vigliani@polito.it

Abstract

This paper deals with the design of a brake caliper pressure controller for a conventional ABS/ESC system and the experimental validation of its tracking performances. The analysis of the hydraulic plant, carried out in Part I of this two-part study, is here utilized to develop the control algorithm for ABS digital electro-hydraulic valves.

The control strategy is based on a Feedforward (FF) and a Proportional Integral (PI) controller through a Pulse Width Modulation (PWM) with constant frequency and variable Duty Cycle (DC). FF contribution requires modeling the nonlinear open-loop system behavior which has been experimentally identified and described through 2-D maps: the inputs are the DC applied to the electro-valves and the pressure drop across their orifice, while the output is the pressure gradient in the brake caliper. These maps, obtained for inlet and outlet valves, are used to set the FF term. Finally a PI controller is designed to reject external disturbances and compensate for model uncertainties.

A brake system test rig, described in Part I, is used for building inverse maps and validating the proposed control logic. Different reference pressure profiles are used to experimentally verify the control tracking performances.

Index Terms

braking system, pressure control, chassis control system, ABS control unit.

I. INTRODUCTION

There are many versions of active braking systems, providing different degrees of braking support. Early systems, such as Brake Assist, measure some variables (e.g., wheel speed, vehicle acceleration and braking pressure) and estimate some others (vehicle velocity) to determine whether the driver is attempting an emergency stop [1], [2]. In case an emergency is detected, the control system applies additional brake pressure in order to enhance the promptness of the braking system, which is somehow limited by the presence of the ABS valves, whose small flow orifices represent a significant obstacle to a quick pressure build-up and produce an undesirable stiffening effect on the brake pedal.

Different control strategies have been proposed in the past for achieving improved braking performance of vehicles during emergency scenarios: Mauer [3] proposes a digital controller which combines a fuzzy logic element and a decision logic network; in [4] an adaptive sliding-mode control is presented for an electro-hydraulic system with nonlinear unknown parameters. A hybrid controller based on the feedback linearization combined with two feed-forward neural networks to face the system nonlinearities is presented in [5]. Moreover, Dash and Subudhi [6] exploit benefits of both fuzzy logic and sliding mode

control in designing a fuzzy adaptive sliding mode control for tyre longitudinal slip ratio regulation on a hybrid vehicle. All these control approaches intend to control the slip ratio aiming at reducing the stopping distance by preventing wheel lockup while simultaneously providing directional control and stability. Other papers propose alternative control strategies based on information coming from new sensors for the measurement of the longitudinal forces at the hub bearings [7], [8].

In the last years, active braking systems have been re-evaluated to be integrated in the design of global chassis control strategies thus not limiting their task to emergency braking maneuvers (i.e. ABS, ESC as mentioned before). More advanced systems have been introduced to use innovative sensors (radar, lidar, camera, etc) to scan ahead of the car for moving and stationary hazards. One example is represented by Collision Warning and Collision Avoidance (CW/CA) systems which are active subjects of research and development by most automotive manufactures around the world due to their potential for increased vehicle safety: if a potential collision is detected, audiovisual warnings are provided to the driver and the brakes are primed ready for maximum application. In this new scenario, the braking system is exploited for following a reference pressure in order to accomplish high level control targets (i.e. collision avoidance) thus moving the control effort from slip ratio to brake caliper pressures. Many analytical and experimental studies on CW/CA strategies have been performed [9]–[13]: most of them have assumed a binary braking logic, i.e., an on/off use of brakes. In [9] a nonlinear brake control law is applied to a CW/CA system, which uses a analogical solenoid-valve-controlled hydraulic brake actuator.

Another important application of braking pressure control is also found in Electro-Hydraulic Braking (EHB) design, which is the key feature of stability control and regenerative braking system for hybrid and electric vehicles [20], [21]. This pressure control is usually related with the application of linear solenoid valves, which are suitable for the task but also quite expensive and not available in conventional internal combustion engine driven cars. A conventional ABS/ESP unit includes a hydraulic pressure modulator with on/off digital valves normally used for slip control and not for the continuous control of the braking pressure inside the calipers. In [14], [15] a detailed electro-mechanical model of an on/off solenoid valve used to regulate brake pressure is presented; due to the valves discontinuous characteristic, PWM is often used to drive both hydraulic [16]–[18] and high-speed pneumatic [19] valves.

In this wide technological context, this paper proposes a new control strategy of a normal-production ABS unit in order to continuously track a reference pressure previously defined (i.e. for CW/CA or EHB strategies). In the literature review, some papers about a continuous pressure following control can be found:

- [9] presents a continuous pressure control based on sliding mode where the on/off valves are modeled as a second order dynamic system;
- in [15] an open-loop controller is designed and the output of the control is the current of the On/Off digital valves instead of its voltage;
- in [18] a PI control has been developed using standard feedback linearization techniques on a nonlinear validated model;
- in EHB applications [20], [21], proportional solenoid valves are used for the pressure following control;

Differently from other literature works,in this paper the controller has been designed from an experiments-based description of brake pressure dynamics for elaborating the FF part and from its linearization for the PI gains selection.

Since ABS valves dynamics is highly nonlinear and characterized by uncertainties, experiments on a Hardware-In-the Loop

Fig. 1. Hydraulic scheme for the raising and falling phase in a brake caliper including Inlet/Outlet valves, Motor-pump and Spring accumulator.

(HIL) Brake System Test bench have been carried out to build an experimental model of ABS on/off valves specifically used for the design of a Feed-Forward (FF) and PI control logic based on PWM regulation of conventional on/off digital valves. The paper is structured as follows: in section II a brief mathematical description of the valves behavior is presented to establish the most influential variables; Section III is related to the methodology used to obtain open-loop maps thus expressing the experimental relation among pressure gradient and DC and pressure drop across each valve; in section IV the control strategy is explained and the inversion of open-loop maps generated in section III is adopted to build the FF contribution; finally section V shows some experimental results from HIL test bench to validate the control logic and section VI reports final conclusions.

II. VALVES DYNAMICS BEHAVIOR

Brake pressure inside calipers can be modulated through the activation of Inlet and Outlet valves. A generic scheme for the 'raising' phase (when brake pressure p_b increases) controlled by the Inlet valve and the 'falling phase' (when brake pressure p_b decreases) managed by the presence of Outlet valve and motor-pump is shown in Fig. 1.

Brake pressure gradient $\dot{p}_b$ is described by the following equation:

$$\dot{p}_b = \frac{\beta}{V_b}(Q_{In} - Q_{Out}) \tag{1}$$

where V_b is the volume of brake caliper, β is the oil bulk modulus and Q_{In}, Q_{Out} are the flow rates respectively through Inlet and Outlet valves that are expressed by:

$$\begin{cases} Q_{In} & = c_{q,In}A_{In}\sqrt{\frac{2|p_T-p_b|}{\rho}}sgn(p_T - p_b) \\ Q_{Out} & = c_{q,Out}A_{Out}\sqrt{\frac{2|p_b-p_a|}{\rho}}sgn(p_b - p_a) \end{cases} \tag{2}$$

where c_q is the flow coefficient, ρ the oil density, p_T the pressure inside one of the TMC chambers, p_a the spring accumulator pressure and A_{In}, A_{Out} Inlet and Outlet nominal flow areas. Under the hypothesis that the two valves cannot be simultaneously

open, when Inlet valve is activated (raising phase) Q_{Out} is null while when Outlet valve is open (falling phase) Q_{In} is equal to zero.

From eqs. (1) and (2), it is evident that the brake pressure depends on flow areas and on pressure drop across the two valves. Inlet valve behavior is described considering as inputs:

- Inlet pressure drop $\Delta p_{In} = p_T - p_b$
- flow area A_{In}

and as output:

- brake calipers pressure gradient $\dot{p}_b$

Also Outlet valve can be represented considering as inputs:

- Outlet pressure drop $\Delta p_{Out} = p_b - p_a$
- flow area A_{Out}

and as output:

- brake calipers pressure gradient $\dot{p}_b$

In this last case, the spring accumulator guarantees a reference pressure for the suction port of the motor-pump. Accumulator pressure p_a is not measured by a sensor but, as higlighted in the Part I of this activity, it is reasonable to approximate the pressure drop across the Outlet valve with the brake pressure p_b alone.

Hence a possible strategy to control the brake pressure gradient is to modulate the valve command thus regulating their flow areas. Since electrovalves are designed to receive a digital command, the generation of a PWM signal as input voltage is a solution to modify in a continuous way their flow area. Meanwhile, pressure drops across valves can be considered as an external disturbances from the control point of view, that are measured on the test bench through sensors placed in the TMC and inside each brake calipers.

A PWM signal is described by a frequency and a Duty Cycle that is the percentage of a modulation period during which the signal is active. By fixing the PWM frequency, the DC is used to change the effective flow area and so to regulate the flow rate going inside/outside the brake caliper thus controlling brake pressure.

III. VALVES CHARACTERIZATION

The test rig used for valves characterization is shown in Fig. 2, where a normal production hydraulic brake system is controlled by a customized ABS/ESC electronic unit to command directly Inlet and Outlet electrovalves together with the motor-pump.

The electronic unit is controlled by means of a dedicated PC running a real-time operating system and equipped with National Instrument software and hardware; the control logic is implemented with Matlab/Simulink and then properly compiled to be executed on a real-time target (NI-PXI). A PWM signal is chosen to command Inlet and Outlet valves meanwhile the motor-pump is activated with an On-Off logic. Calipers brake pressure and TMC pressures are here considered measurable and available feedback for the proposed pressure controller.
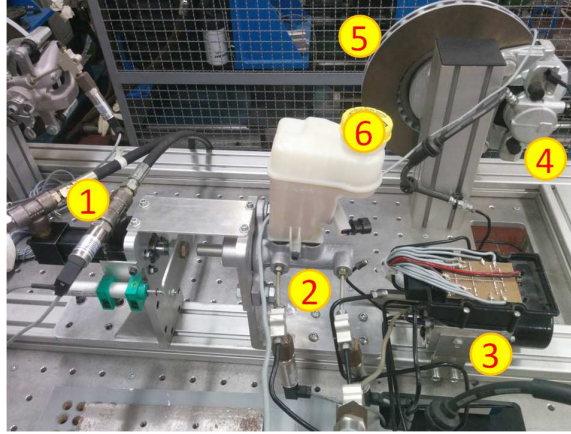
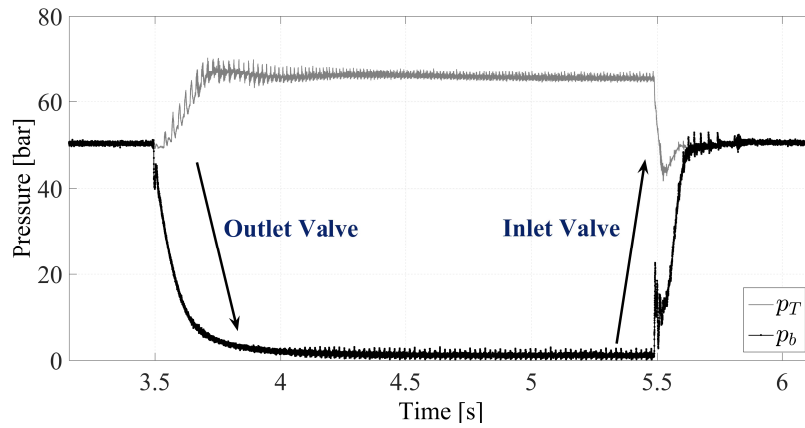Fig. 2. HIL Test Rig 1-Hydraulic cylinder 2-TMC 3-customized ESC 4-Brake caliper 5-Brake disk 6-oil tank

Fig. 3. Data Acquisition with a sample time of 0.1 ms of TMC (p_T) and Brake (p_b) pressures

A more refined analysis of the valves can be achieved through a semi-empirical model by involving experimental maps to describe their dynamics. An experimental test is carried out to analyze valves response to a PWM signal: starting from a steady-state condition where all valves are in their normal configuration (normally open for Inlet and normally close for Outlet) and brake pressure p_b is equal to TMC pressures, the brake caliper it is emptied by applying a PWM signal with a certain frequency and DC to the Outlet valve (together with the activation of the motor-pump) while the Inlet valve is kept closed; when brake pressure p_b falls below a specific software selectable threshold, i.e. 5 bar, the Inlet valve is excited with a PWM signal in order to increase brake pressure while Outlet valve is closed and motor-pump is switched off. This cycle of 'falling' and 'raising' phases is repeated when the brake pressure has reached again the TMC pressure.

An example of a data acquisition is presented in Fig. 3 where different duty cycles are imposed for Inlet (30%) and Outlet (55%) valves with the same PWM frequency of 900 Hz.

The figure also shows how valves activation influences the brake and TMC pressures since their variation has a direct effect on the flow rate (and so on the gradient of brake pressure). The correlation between PWM command and valves behavior will be fully described by experimental maps obtained by choosing a suitable value of PWM frequency and a DC range within which brake pressure gradient is controllable.
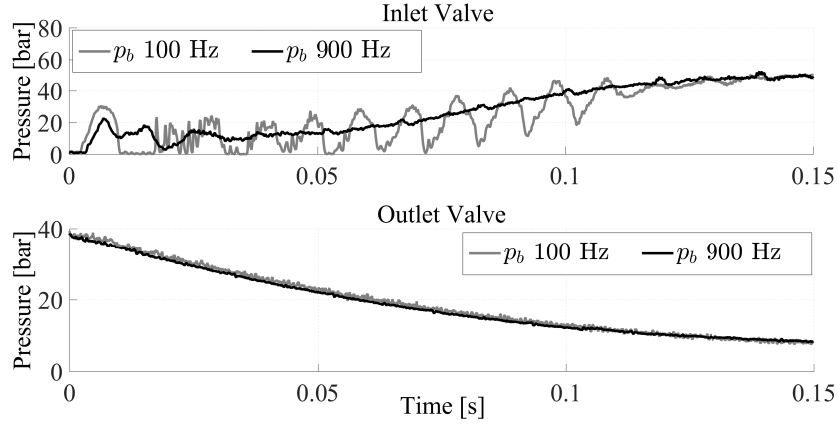
Fig. 4. PWM signal with different frequencies for both Inlet (DC=30%) and Outlet Valves (DC=70%), p_b = Brake Pressure

A. PWM Frequency selection

Starting from a preliminary test, a PWM command with a constant duty cycle and different frequencies (range between 50 and 900 Hz) is applied to both valves in order to choose a suitable frequency for the control strategy. By exciting the Inlet valve with a PWM command characterized by a DC of 30% and a frequency of 100 Hz, lower with respect to Fig. 3, a different behavior can be observed as shown in Fig.4: a PWM frequency smaller than 100 Hz leads to significant pressure oscillations.

PWM frequency directly influences brake pressure ripples so it can be selected in order to reduce oscillations and to improve pressure controllability. The Root Mean Square (RMS) of the difference between raw and filtered signal (zero-phase digital filter with a cut-off frequency of 15 Hz) is used to correlate the ripple pressure to the PWM frequency:

$$P_{RMS} = \sqrt{\frac{\sum_{i=1}^{n}(p_{bi} - p_{bfi})^2}{n}} \tag{3}$$

where P_{bi} is the raw pressure and P_{bfi} its value filtered at time t_i. Fig. 5 shows that the pressure ripple for Inlet valve decreases with the PWM frequency and after 500 Hz this trend is settled. This means that a high frequency could lead to a better solution in terms of controllability by cutting off the PWM frequency content which is a disturbance for pressure control. Outlet valve shows a decreasing trend similar to the Inlet one, with a noticeable difference in terms of RMS amplitude range: it is less influenced by PWM modulation frequency than Inlet valve, as visible in Fig.5. This behavior can be explained considering that the pressure oscillations in the outlet branch are influenced both by PWM frequency content and by the motor-pump which is not present in the inlet branch. Consequently the motor-pump can be considered as a flow-rate regulator which modifies the pressure oscillations caused by the PWM command.

Finally PWM frequencies of 900 Hz and 50 Hz are chosen for Inlet and Outlet valves respectively, aiming at obtaining the minimum pressure ripple according to Fig. 5.

Since the brake pressure dynamics is minimally affected by the outlet valve PWM frequency, the selection of this parameter for the outlet valve is aimed at obtaining the max DC range which is effective during pressure control as it will be seen in
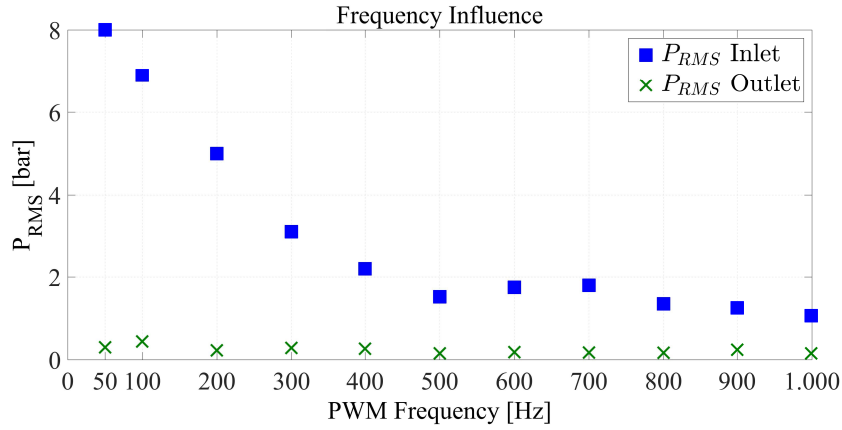
Fig. 5. PWM frequency influence on brake pressure ripple for both Inlet (blue) and Outlet (green) valves
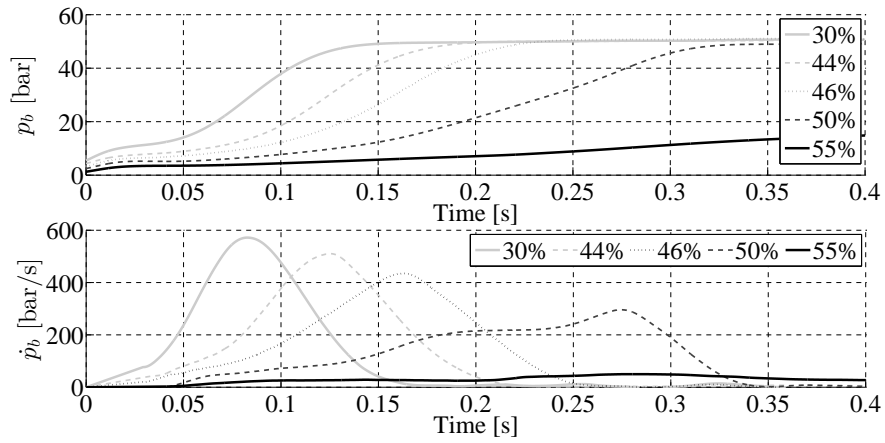

Fig. 6. Brake pressure (up) and its gradient (down) vs time for different values of DC (Inlet valve)

next section.

B. DC range: Open-loop Maps

The relation between DC and pressure gradient is not linear and it is limited within a certain range beyond which the duty cycle no longer affects the pressure dynamics. A first step refers to the search for a duty cycle range to achieve a good sensitivity in terms of controllability within minimum and maximum DC. A gradual variation of the duty cycle is applied to each valve (by keeping PWM frequency as indicated in the previous section) in order to build up the open-loop maps describing the experimental relationship between input (DC) and output ($\dot{p}_b$).

By considering the Inlet valve (normally open), the pressure gradient decreases with increasing DC until the valve is not able to further increase pressure because the opening time is too short, as it happens when a DC of 55% is imposed with a nominal frequency of 900 Hz (Fig. 6). If DC is larger than 55%, pressure cannot be increased up to TMC pressure thus representing maximum limit for Inlet valve. DC minimum limit can be evaluated from the same experimental data when the valve behaves as a fully open one (a lower DC is ineffective), thus getting a complete information about valves open-loop behavior.

Fig. 6 indicates that for a fixed DC, pressure gradient is not constant since it depends also on the pressure drop across the valve $\Delta p_{In} = p_T - p_b$, which is measurable on the test rig. Therefore, an experimental relationship between pressure gradient
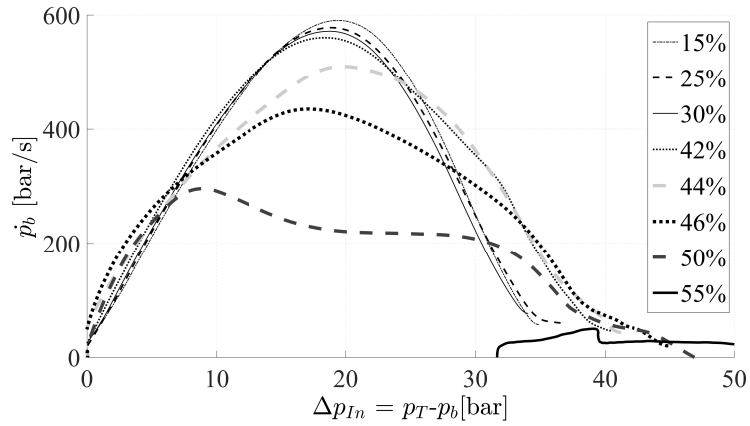
Fig. 7. Inlet Open-Loop map: pressure gradient vs pressure drop across Inlet valve for different value of DC

$\dot{p}_b$, pressure drop Δp_{In} and *DC* is obtained, which constitutes the open-loop map of Inlet valve (Fig. 7).

The 'bell' shape in Fig. 7 can be divided into three sections: the increasing section, the peak point and decreasing section. The increasing section and peak point show an almost inversely proportional trend with respect the DC: the pressure gradient in brake caliper decreases consequently to a reduction of the inlet valve effective flow area due to an increase of DC.

The behavior of the system corresponding to the decreasing section cannot be explained in the same way, due to the saturation limit imposed by the TMC pressure (without this limit, the decreasing section would not be present): it is not intuitive to figure out how the DC influences the pressure gradient. It is of interest noting that in the DC operative range there exists a progressive modulation of pressure gradient with respect to DC, thus becoming a feasible controllable variable.

Figures 6 and 7 clearly show the upper and lower limits of duty cycle range for the Inlet valve; under the lower limit, a packing effect of the curves occurs: pressure gradient is no more influenced by DC (the same behavior of a fully open valve) and a transition occurs between the active (where a variation of DC provokes a variation of pressure gradient) and the passive region (where pressure gradient is not influenced anymore by the DC): this transition modifies the 'bell' shape, causing an intersection of the curves in the decreasing section. In Fig. 7 can be seen that DC of 15%, 25% and 30% have the same bell shape meanwhile a DC of 42% has a shape which is a sort of composition of 30% and 44% DC curves.

Similarly, the Outlet open-loop map is built selecting the appropriate duty cycle range between upper and lower limits, considering that the outlet valve is normally closed (when DC is too low the valve behaves as a fully close one) and that the pressure drop across the valve, $\Delta p_{Out} = p_b - p_a$, is approximated with the brake pressure p_b (neglecting the influence of spring accumulator). The open-loop map obtained for the Outlet valve is reported in Fig. 8.

IV. CONTROL LOGIC DESIGN

A non-linear FeedForward (FF) plus a Proportional Integral (PI) controller is designed for continuously tracking a reference pressure which can be generated, for example, by a high-level control logic aiming at a global chassis control. In order to design the controller structure and to figure out its performance enhancement, a linearization around a nominal equilibrium point is required. Equilibrium points can be found just starting from dynamic equations that describe brake pressure behavior for both inlet and outlet valves in Eq. 1,2:
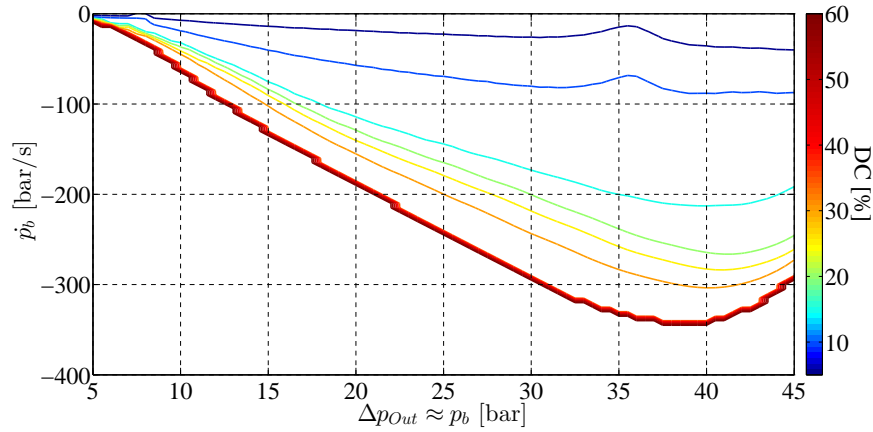
Fig. 8. Outlet Open-Loop map: pressure gradient vs pressure drop across Outlet valve for different value of DC

$$\dot{p}_{b,In}(p_b, A_{In}, p_T) = \frac{\beta}{V_b} c_q A_{In}(DC_{In}, \Delta p_{In}) \sqrt{\frac{2\Delta p_{In}}{\rho}} \tag{4}$$

$$\dot{p}_{b,Out}(p_b, A_{Out}) = -\frac{\beta}{V_b} c_q A_{Out}(DC_{Out}, p_b) \sqrt{\frac{2p_b}{\rho}} \tag{5}$$

where A_{In} and A_{Out} depends on DC and pressure drop across each valve. Steady-state occurs when $\dot{p}_b = 0$: a trivial solution is obtained when $p_{T,n} = p_{b,n}$ for Inlet hydraulic branch and $p_{b,n} = 0$ for Outlet hydraulic branch.

A more interesting steady-state condition is reached when $A_{In,n} = 0$ ($DC_n = 100\%$) $\forall \Delta p_{In,n} = (p_T - p_b)_n$ for Inlet valve and $A_{Outlet,n} = 0$ ($DC_n = 0\%$) $\forall p_{b,n}$ for Outlet valve. This means that any value of brake pressure p_b represents a stable configuration when $A_{Out,n} = 0$ and $A_{In,n} = 0$.

Since pressure gradient in equations Eq.4 and Eq.5 is a function of two variables (DC and Δ_p), the following linear relations are obtained respectively for Inlet and Outlet hydraulic branches, by linearizing around nominal equilibrium points:

$$\dot{p}_{b,In} = \frac{\partial \dot{p}_{b,In}}{\partial DC_{In}}\bigg|_n (DC_{In} - DC_{In,n}) + \frac{\partial \dot{p}_{b,In}}{\partial \Delta p_{In}}\bigg|_n (\Delta p_{In} - \Delta p_{In,n}) = k_{DC,In}(DC_{In} - DC_{In,n}) + k_{\Delta,In}(\Delta p_{In} - \Delta p_{In,n}) \tag{6}$$

$$\dot{p}_{b,Out} = -\frac{\partial \dot{p}_{b,Out}}{\partial DC_{Out}}\bigg|_n (DC_{Out} - DC_{Out,n}) + \frac{\partial \dot{p}_{b,Out}}{\partial p_b}\bigg|_n (p_b - p_{b,n}) = k_{DC,Out}(DC_{Out} - DC_{Out,n}) + k_{\Delta,Out}(p_b - p_{b,n}) \tag{7}$$

Eq. 6 and 7 state that brake pressure gradient is influenced by DC of valve input signal and pressure drop across valves through four coefficients $k_{DC,In}$, $k_{DC,Out}$, $k_{\Delta,In}$ and $k_{\Delta,Out}$. These two relations, neglecting the constant terms, can be grouped in a unique general formulation for both inlet and outlet valves:

$$\dot{p}_b = k_{DC}DC + k_\Delta \Delta p = k_{DC}DC + k_\Delta p_T - k_\Delta p_b \tag{8}$$

where $DC = DC_{In}$ for inlet valve, $DC = -DC_{Out}$, $k_\Delta p_T = 0$ for outlet valve and k_{DC}, k_Δ are linearization coefficients related to nominal equilibrium points.

By applying Laplace transform to Eq. 8, it is possible to derive the transfer function between output p_b and input (DC,p_T):

$$p_b(s) = \frac{k_{DC}}{s+k_\Delta}DC(s) + \frac{k_\Delta}{s+k_\Delta}p_T(s) \tag{9}$$

where s is the Laplace variable and DC is the controlled input p_T represents a measurable disturbance. The poles of transfer function (9) depend on coefficient k_Δ which states the relation between $\dot{p}_b$ and the pressure drop across each valve and it is expressed by the gradient of open-loop maps when DC is fixed to a constant value. For both inlet and outlet valves k_Δ changes from positive (stability region) to negative (instability region) values: by looking the Inlet open-loop map (Fig. 7), for high pressure drops (right side of the map with a negative k_Δ), an increase in pressure causes an increase of pressure gradient, making the linearized system unstable. On the other hand, for low pressure drops (left side of the map with a positive k_Δ), the system shows a stable behavior.

The Control logic used to stabilize the system and to track the reference brake pressure is composed of two different contributions:

- a non-linear FeedForward (FF) part which is based on dynamics system inversion of the open-loop behavior;
- a Proportional-Integrative (PI) part which aims to reject noise and to compensate for model parameters uncertainties not considered in the FF contribution.

A. Feed Forward Controller

A FF contribution is built by considering the dynamics of brake pressure gradient: it works to track the gradient of the reference pressure. Theoretically speaking, this is obtained inverting Eq. 8:

$$DC_{FF} = \frac{\dot{p}_r - k_\Delta(p_T - p_b)}{k_{DC}} \tag{10}$$

where $\dot{p}_r$ is the gradient of the reference brake pressure. Since gains k_Δ and k_{DC} are not constant in the real system, dynamics inversion can be easily achieved by inverting experimental open loop maps $\dot{p} = f(DC, \Delta p)$ to inverse maps $DC = f(\dot{p}, \Delta p)$ through a post-processing procedure consisting of two phases:

1) Original maps discretization & interpolation: each pressure gradient trend in Fig. 7 and Fig. 8 has a different x-axis (pressure drop across valves) discretization, thus requiring a suitable standardization which is obtained by fixing a common abscissa distribution. Consequently, a linear interpolation is carried out to create a common x-axis discretization and to fill original open-loop maps where experimental values are not available, providing more data for the following inversion step.

2) Maps inversion: for each pressure drop Δp there exists an experimental correlation between pressure gradient and duty cycle: hence a simple vector inversion is performed as shown in Fig. 9.

Finally, Fig. 10 and 11 illustrate the inverse maps for Inlet and Outlet valves, respectively.

It is important to highlight that DC_{FF} is not a traditional open-loop feedforward since inverse maps use as input feedback from the plant, the actual pressure drop across valves measured by sensors whose effect will be clarified in the next subsection.
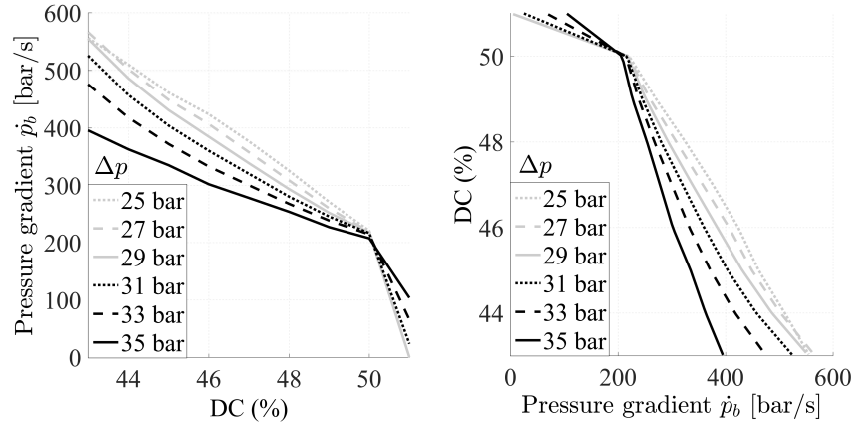
Fig. 9. Conversion from open-loop map (left) to inverse map (right) for different values of pressure drop across Inlet valve
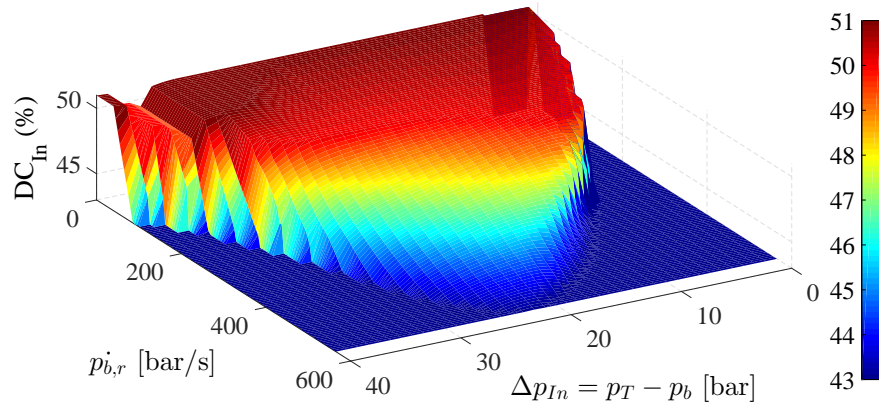

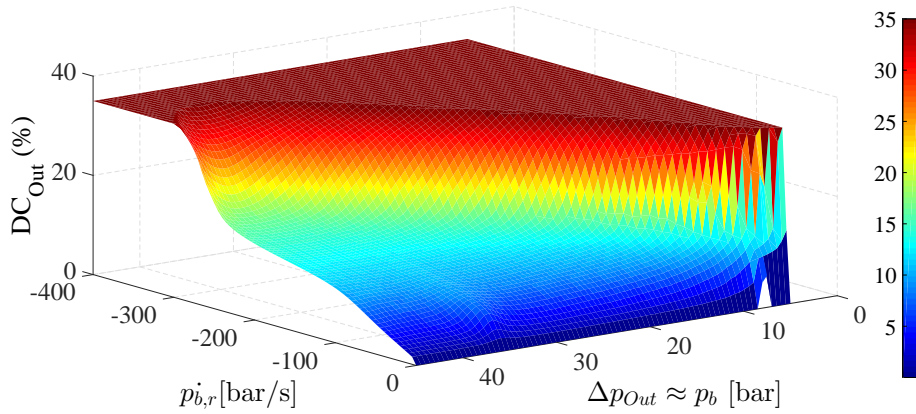Fig. 10. Inlet Inverse map: DC vs reference pressure gradient and pressure drop across Inlet valve

Fig. 11. Outlet Inverse map: DC vs reference pressure gradient and pressure drop across Outlet valve

B. Proportional Integrative Controller

Open-loop maps are obtained from experimental data, so they are obviously affected by uncertainties. In order to reduce their impact on the control strategy and to better track the reference brake pressure, a PI controller on the error between p_b and $p_{b,r}$ is designed.
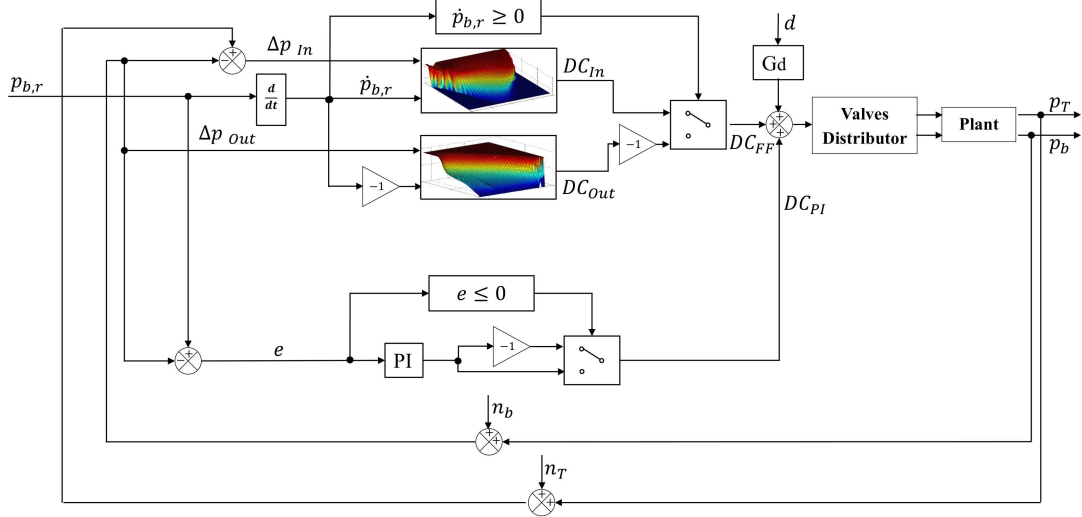
Fig. 12. Block diagram of FF + PI control strategy

In order to understand the PI effects on the closed loop system shown in Fig. 12, a not measurable disturbance d is added to the control output $u_c = DC_{FF} + DC_{PI}$ and sensor noises n_b, n_T are considered respectively for both TMC and brake pressures. Pressure gradient equation express in Eq. 8 is modified as:

$$\dot{p}_b = k_{DC}DC + k_\Delta p_T - k_\Delta p_b + G_d(s)d \tag{11}$$

By considering the Laplace transform of 11, a new transfer function of the disturbed plant is obtained:

$$p_b(s) = \frac{k_{DC}}{s + k_\Delta}DC(s) + \frac{k_\Delta}{s + k_\Delta}p_T(s) + \frac{G_d(s)}{s + k_\Delta}d(s) \tag{12}$$

The closed loop transfer function from $p_{b,r}$ to p_b can be derived considering the controller equations $DC(s)$

$$DC(s) = DC_{PI}(s) + DC_{FF}(s) = (K_{Pr} + \frac{K_{In}}{s})e(s) + DC_{FF}(s) \tag{13}$$

where $e(s) = p_{b,r} - p_b - n_b$, K_{Pr} is the proportional gain, K_{In} is the integral gain and DC_{FF} is the DC from inverse maps. Finally, the relation between the output $p_b(s)$ and the input $p_{b,r}(s), p_T(s), d(s), n_b(s)$ is calculated by substituting Eq.13 in Eq.12:

$$p_b(s)\left(1+K_{Pr}\frac{k_{DC}}{s+k_\Delta}+\frac{K_{In}}{s}\frac{k_{DC}}{s+k_\Delta}\right)=\left(K_{Pr}\frac{k_{DC}}{s+k_\Delta}+\frac{K_{In}}{s}\frac{k_{DC}}{s+k_\Delta}\right)p_{b,r}(s)+$$
$$+\left(\frac{k_{DC}}{s+k_\Delta}DC_{FF}(s)\right)+\left(\frac{k_\Delta}{s+k_\Delta}\right)p_T(s)+\left(\frac{G_d(s)}{s+k_\Delta}\right)d(s)-\left(K_{Pr}\frac{k_{DC}}{s+k_\Delta}+\frac{K_{In}}{s}\frac{k_{DC}}{s+k_\Delta}\right)n_b(s)$$

$$\tag{14}$$

Without considering the effect of $DC_{FF}(s)$, this equation shows how PI gains can modify the closed loop transfer function between $p_b(s)$ and $p_{b,r}(s)$. On the other hand, DC_{FF} derives from inversion of the nominal open-loop dynamic behavior, see Eq. 10 hence Laplace transform is:

$$DC_{FF}(s)=\frac{s}{k_{DC}}p_{b,r}(s)-\frac{k_\Delta}{k_{DC}}p_T(s)-\frac{k_\Delta}{k_{DC}}n_T(s)+\frac{k_\Delta}{k_{DC}}p_b(s)+\frac{k_\Delta}{k_{DC}}n_b(s) \tag{15}$$

by substituting Eq. 15 in Eq. 14 it yields:

$$p_b(s)=p_{b,r}(s)-\left(\frac{(k_{DC}K_{Pr}+k_\Delta)s+k_{DC}K_{In}}{s^2+k_{DC}K_{Pr}s+k_{DC}K_{In}}\right)n_b(s)-\left(\frac{k_\Delta s}{s^2+k_{DC}K_{Pr}s+k_{DC}K_{In}}\right)n_T(s)+\left(\frac{G_d(s)s}{s^2+k_{DC}K_{Pr}s+k_{DC}K_{In}}\right)d(s) \tag{16}$$

and in terms of tracking error $e(s)$:

$$e(s)=\left(\frac{k_\Delta s-s^2}{s^2+2\zeta\omega_n s+\omega_n^2}\right)n_b(s)+\left(\frac{k_\Delta s}{s^2+2\zeta\omega_n s+\omega_n^2}\right)n_T(s)-\left(\frac{G_d(s)s}{s^2+2\zeta\omega_n s+\omega_n^2}\right)d(s) \tag{17}$$

where

$$\omega_n=\sqrt{k_{DC}K_{In}}$$
$$\zeta=\frac{K_{Pr}}{2}\sqrt{\frac{k_{DC}}{K_{In}}} \tag{18}$$

Non-linear FF is able to improve control tracking performance ($\frac{p_b(s)}{p_{b,r}(s)}=1$) and reject the measurable disturbance p_T, but it is not able to reject unmeasurable disturbances like d and sensor noises like n_T,n_b. The intervention of the PI control is able to modify the poles of transfer functions $\frac{e(s)}{n_b(s)}$, $\frac{e(s)}{n_T(s)}$ and $\frac{e(s)}{d(s)}$ thus enhancing robustness against uncertainties and external disturbances. Considering firstly the transfer function $\frac{e(s)}{n_T(s)}$, without a PI controller ($K_{Pr}=0$ and $K_{In}=0$) only one pole in zero is present: in the low frequency range, TMC pressure sensor noises can negatively affect error between brake pressure and its reference value. The presence of proportional and integral gains can change the position of close-loop poles: by considering a fixed value of k_Δ and k_{DC}, bode plots of $\frac{e(s)}{n_T(s)}$ and $\frac{e(s)}{n_b(s)}$ for different values of K_{Pr} and K_{In} are compared in Fig. 13. Integral gain modify the Bode plot magnitude on the low frequency region and implies a resonance amplitude peak which can be reduced by the proportional gain. Eq. 17: proportional gain influences damping factor (ζ) since integral gain is selected to modify natural frequency (ω_n).
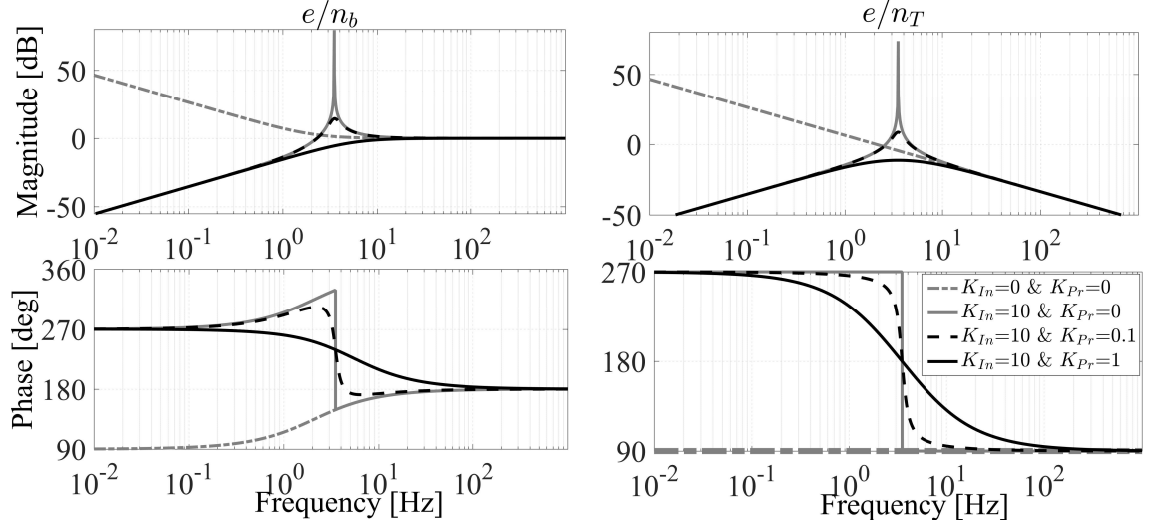
Fig. 13. Bode plots for transfer functions $\frac{e(s)}{n_b(s)}$ (left) and $\frac{e(s)}{n_T(s)}$ (right)
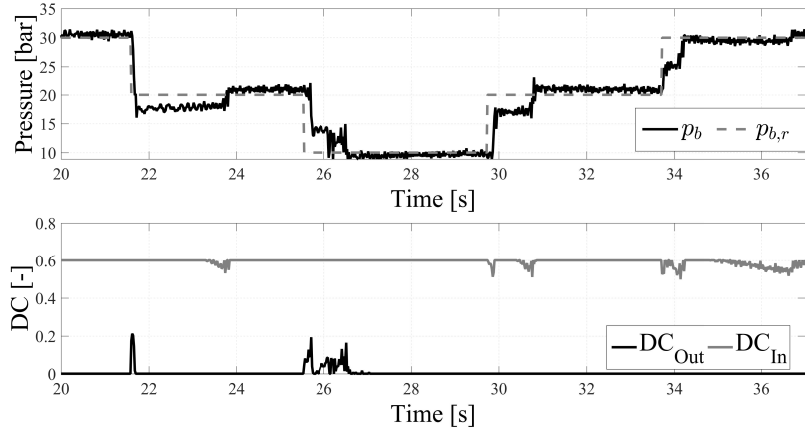

Fig. 14. System response to a sequence of step changes of the reference pressure (dashed gray)

V. EXPERIMENTAL RESULTS

Last part of the paper shows the experimental results obtained applying the proposed controller to the physical system on the test rig. The update rate of the controller set during the experiments is 50 Hz. This limitation is due to the PWM frequency selected for the outlet valve (50 Hz): the electronic instrumentation used for controlling/monitoring the braking system is not able to generate a PWM signal with a frequency lower than the sampling rate of the controller. System responses to three different stimulus profiles are proposed, in order to show the accuracy and efficacy of the proposed controller.

A. Step response

Starting from $K_{Pr} = 1$, $K_{In} = 10$ as optimal values in Fig. 13, a sequence of constant steps is imposed to the reference pressure signal in order to validate PI gains.

Fig. 14 shows the closed-loop system response, where reference pressure is tracked quite precisely. In this first experiment, FF term intervenes only in the time interval between one step and the following ($\dot{p}_{b,r} \neq 0$), since the required pressure gradient is null when the reference pressure is constant.
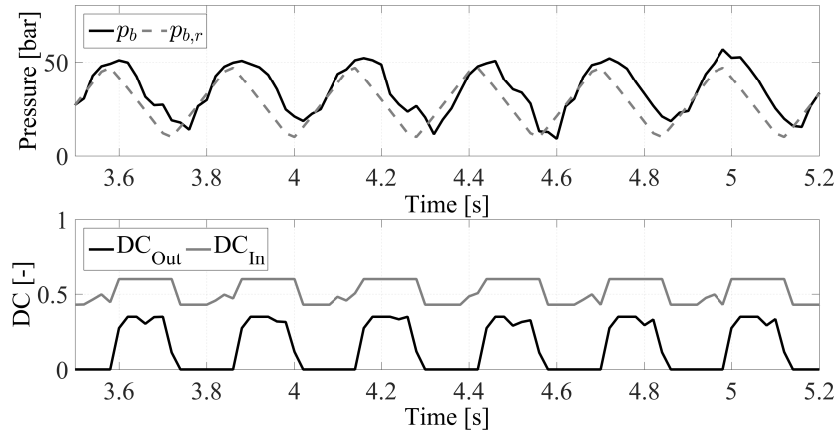
Fig. 15. System response to a triangle wave reference pressure (dashed gray)
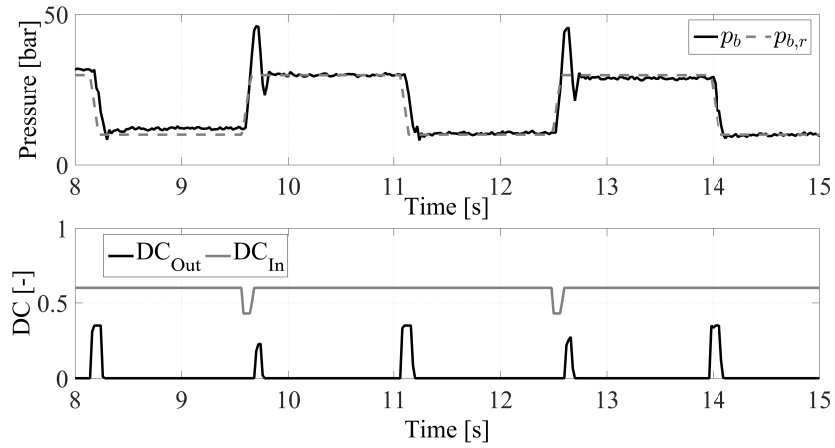

Fig. 16. System response to a trapezoidal wave reference pressure (dashed gray)

It is of interest observing that when brake pressure reaches the reference value, both valves stay closed keeping the pressure equal to its reference value. The lower subplot of Fig. 14 shows valves DC in their control operative range: the Inlet DC saturates at 60%, since it behaves as a fully closed valve for larger DC.

B. Triangle wave excitation

A second experiment is performed by imposing a triangle wave signal to the reference pressure. This experiment allows evaluating the FF contribution, i.e. how inverse maps work in response to a constant reference pressure gradient (the PI control is disabled during this test). The response is plotted in Fig. 15: even though the measured pressure does not closely match the reference, due to the absence of the linear feedback controller, its gradient closely resemble the 300 bar/s imposed by the wave. The lower chart highlights the activation of both valves in their respective DC operative range: DC values are obtained by entering the inverse maps with $\dot{p} = \pm 300$ bar/s.

C. Trapezoidal excitation

Finally, a trapezoidal excitation allows appreciating the intervention of both FF and PI terms.

Fig. 16 proves that the use of inverse maps integrated with a PI controller leads to noticeable improvement in following the reference pressure. PI contribution has the double effect of controlling brake pressure when $\dot{p} = 0$ without adopting FF inverse maps (switching between Inlet and Outlet valve in order to keep constant the brake pressure) and to rejects external disturbances when FF is activated ($\dot{p} \neq 0$). The overshoot visible in figure could be limited by adopting a faster control loop rate; unfortunately, as previously stated, the experimental system does not allow to further increase this parameter (the limit is 50 Hz).

VI. CONCLUSION

The paper presents a methodology to analyze and characterize the dynamic behavior of a commercial ABS control unit commonly present on passenger cars. Oil pressure dynamics inside brake calipers is described by open-loop maps which represent the experimental relation between pressure gradient and pressure drop across valves and DC command.

Experiments were run on a dedicated test bench to characterize the valve dynamics, thus allowing to choose an appropriate frequency and duty cycle range and to build open loop maps.

A FF + PI strategy based on the control of PWM DC for each valve (inlet & outlet) is implemented in order to track a desired reference brake pressure: FF contribution is calculated from inversion of open-loop maps and PI contribution is used to close the loop on the brake pressure rejecting external disturbances and sensor noises.

Finally three different experimental tests are used for control logic validation and evaluation of control performances. Experimental results prove the effectiveness of FF + PI control technique for vehicle global chassis control logic using a common automotive brake system.

VII. LIST OF SYMBOLS

a : subscript relative to spring accumulator

A_i : flow area of ith hydraulic resistance

b : subscript relative to Rear-Right brake caliper

c_q : flow Coefficient

d : external disturbance

DC : Duty Cycle of a PWM signal

e : error between reference and actual pressure

In : subscript relative to inlet valve

K_{Pr} : proportional gain

K_{In} : integral gain

n : subscript relative to a nominal conditionv

n_i : noise on the ith measure

Out : subscript relative to outlet valve

p : subscript relative to pump

p_i : pressure of ith hydraulic branch

Q_i : flow rate across the ith hydraulic resistance

r : subscript relative to reference signal

s : Laplace variable

T : subscript relative to one TMC chamber

TMC : Tandem Master Cylinder

V_i : volume of ith hydraulic capacity

β : oil + pipe equivalent bulk modulus

Δp_i : pressure drop across the ith valve

ζ : damping factor

ρ : oil density

ω_n : natural frequency

REFERENCES

[1] R. Bosch. GmbH, *Bosch Automotive Handbook*, 7th ed.   Plochingen, Germany, 2007.

[2] R. Bosch. GmbH, *Anti-lock brakes system specification*,   Plochingen, Germany, 2005.

[3] G. F. Mauer, *A Fuzzy Logic Controller for an ABS Braking System*,   IEEE Transactions on Fuzzy Systems, Vol. 3(4), pp. 381-388, 1995.

[4] C. Guan, S. Pan, *Adaptive sliding mode control of electro-hydraulic system with nonlinear unknown parameters*,   Control Engineering Practice, Vol. 16, pp. 1275-1284, 2008.

[5] A. Poursamad, *Adaptive feedback linearization control of antilock braking system using neural networks*,   Mechatronics, Vol. 19, pp. 767-773, 2009.

[6] B. K. Dash, B. Subudhi, *A Fuzzy Adaptive Sliding Mode Slip Ratio Controller of a HEV*,   IEEE International Conference on Fuzzy Systems, Hyderabad, 2013.

[7] D. Capra, E. Galvagno, V. Ondrak, B. van Leeuwen, A. Vigliani, *An ABS control logic based on wheel force measurement*,   Vehicle System Dynamics, Vol. 50(12), pp. 1779-1796, 2012.

[8] A. Morgando, M. Velardocchia, A. Vigliani, V. Ondrak, B. van Leeuwen, *An alternative approach to automotive ESC based on measured wheel forces*, Vehicle System Dynamics, Vol. 49(12), pp. 1855-1871, 2011.

[9] K. Yi, J. Chung*Nonlinear Brake Control for Vehicle CW/CA Systems*,   IEEE/ASME Transactions on Mechatronics, Vol. 6(1), pp. 17-25, 2001.

[10] P. Seiler, B. Song, K. Hedrick, *Development of a collision avoidance system*,   SAE Congress, 98PC-417, Detroit, 1998.

[11] Y. Fujita, K. Akuzawa, M. Sato, *Radar brake system*,   Proc. 1995 Annu. Meeting ITS America, Vol. 1, pp. 95-101, Washington DC, March 1995.

[12] A. Doi, T. Butsuen, T. Niibe, T. Yakagi, T. Yamamoto, H.Seni, *Development of a rear-end collision avoidance system with automatic braking control*, JSAE Rev., Vol. 15(4), pp. 335-340, 1994.

[13] H. J. Asher, B. A. Galler, *Collision Warning Using Neighboring Vehicle Information*,   Proceedings of the 1996 Annual Meeting of ITS America, Washington DC, pp. 674-684, 1996.

[14] M. Branciforte, A. Meli, G. Muscato, D. Porto, *ANN and Non-Integer Order Modelling of ABS Solenoid Valves*,   IEEE Transactions on Control Systems Technology, Vol. 19(3), 2011.

[15] C. Lv, J. Zhang, Y. Li, D. Sun, Y. Yuan, *Hardware-in-the-loop simulation of pressure-difference-limiting modulation of the hydraulic brake for regenerative braking control of electric vehicles*,   Journal of Automobile Engineering, Vol. 228(6), pp. 649-662, 2014.

[16] S. Choi, D. Woo Cho, *Control of Wheel Slip Ratio Using Sliding Mode Controller with Pulse Width Modulation*,   Control of Wheel Slip Ratio Using Sliding Mode Controller with Pulse Width Modulation, Vol. 32, pp. 267-284, 1999.

[17] M. Wu, M. Shih, *Simulated and experimental study of hydraulic anti-lock braking system using sliding-mode PWM control*,   Mechatronics, Vol. 13, pp. 331-351, 2003.

[18] H. Raza, Z. Xu, B. Yang, P. A. Ioannou, *Modeling and Control Design for Computer-Controlled Brake System*,   IEEE Transactions on Control Systems Technology, Vol. 5(3), pp. 279-296, 1997.

[19] J. Wang, B. Yang, S. Li, D. Zhang, k. Li, *Pneumatic electronic braking assistance system using high-speed valves*,   Int. Conf. on Vehicular Electronics and Safety (ICVES), QingDao, 2010.

[20] D. Wu, H. Ding, K. Guo, Z. Wang, *Experimental Research on the Pressure Following Control of Electro-hydraulic Braking system*,   SAE Congress, Detroit, April 2014.

[21] L. Chu, L. Yao, J. Chen, L. Chao, J. Guo, Y. Zhang, M. Liu, *Integrative Braking Control System for Electric Vehicles*,   IEEE Vehicle Power and Propulsion Conference (VPPC), Chicago, 2011.

[22] M. Velardocchia, A. Sorniotti, *Hardware-In-the-Loop to Evaluate Active Braking System Performance*,   SAE Technical Paper, 2005-01-1580, 2005.

[23] M. Velardocchia, *A Methodology to Investigate the Dynamic Characteristics of ESP and EHB Hydraulic Units*,   SAE Technical Paper, 2006-01-1281, 2006.

[24] L. Petrucelli, M. Velardocchia, A. Sorniotti, *Electro-Hydraulic Braking System Modelling and Simulation*,   SAE Technical Paper, 2003-01-3336, 2003.